Applied Physics Letters ARTICLE scitation.org/journal/apl

Thermionic emission or tunneling? The universal transition electric field for ideal Schottky reverse leakage current: A case study in β-Ga_2O_3

Cite as: Appl. Phys. Lett. **117**, 222104 (2020); doi: 10.1063/5.0029348
Submitted: 11 September 2020 · Accepted: 14 November 2020 ·
Published Online: 1 December 2020

View Online Export Citation CrossMark

Wenshen Li,[1] Kazuki Nomoto,[1] Debdeep Jena,[1,2,3] and Huili Grace Xing[1,2,3,a)]

AFFILIATIONS

[1]School of Electrical and Computer Engineering, Cornell University, Ithaca, New York 14853, USA
[2]Department of Materials Science and Engineering, Cornell University, Ithaca, New York 14853, USA
[3]Kavli Institute at Cornell for Nanoscale Science, Cornell University, Ithaca, New York 14853, USA

Note: This paper is part of the Special Topic on Ultrawide Bandgap Semiconductors.
[a)]**Author to whom correspondence should be addressed:** grace.xing@cornell.edu

ABSTRACT

The reverse leakage current through a Schottky barrier transitions from a thermionic emission-dominated regime to a barrier tunneling-dominated regime as the surface electric field increases. In this study, we evaluate such a transition electric field (E_T) in β-Ga_2O_3 using a numerical reverse leakage model. E_T is found to depend on temperature but has an extremely weak dependence on the doping concentration and the barrier height; as a result, a simple empirical expression can be derived to capture this near-universal dependence of E_T on temperature. With the help of a field-plate design, we observed experimentally in lightly doped Ga_2O_3 Schottky barrier diodes near-ideal bulk reverse leakage characteristics, which match well with our numerical model and that confirm the presence of the transition region. Near the transition electric field, both thermionic emission and barrier tunneling should be considered. This study provides important guidance toward accurate design and modeling of Schottky barrier diodes, which can be readily extended to other semiconductors.

With a unique combination of an ultra-high breakdown electric field of ~8 MV/cm,[1,2] a decent electron mobility of ~200 $cm^2/V{\cdot}s$,[3] an availability of melt-grown substrates,[4] and controllable n-type doping,[5] β-Ga_2O_3 is an attractive ultra-wide bandgap semiconductor material for applications demanding high power handling capability.[6] To date, promising performance in Ga_2O_3 devices has been demonstrated, including Schottky barrier diodes with a breakdown voltage (BV) over 2 kV,[7–9] high-voltage power transistors,[10–12] and RF transistors.[13,14]

Ga_2O_3 Schottky barrier diodes (SBDs) are highly versatile. They can be used as high-speed rectifiers for efficient power regulation[15–17] and also function as UV photodetectors.[18,19] In addition, a Schottky contact is a key device building block, offering gate control for metal-semiconductor field-effect transistors (MESFETs),[1] as well as serving potentially as a p–n junction replacement for high field management.[20,21]

Central among all the aforementioned functionalities is the reverse blocking capability of the Schottky barrier, which is critically dependent on the reverse leakage current. In general, the ideal total reverse leakage current ($J_{R,tot}$) through a Schottky barrier consists of the transport of electrons both above and below the top of the barrier. The former mechanism is thermionic emission (TE), while the latter is barrier tunneling (BT), which comprises thermionic-field emission (TFE) and field emission (FE).[22,23] As a result, $J_{R,tot}$ can be expressed as

$$J_{R,tot} = J_{TE} + J_{BT}, \tag{1}$$

where J_{TE} is the thermionic emission current and J_{BT} the barrier tunneling current.

It has been widely recognized that, at a certain temperature, there should exist a transition voltage (V_T) or transition electric field (E_T), below which TE dominates and above which BT dominates.[22,23] E_T is defined as the surface electric field where $J_{TE} = J_{BT}$, while V_T is defined as the corresponding reverse-bias voltage. Knowledge about V_T or E_T is highly valuable since it determines the appropriate bias or electric field ranges for TE and BT models. However, due to the difficulty in calculating the tunneling current analytically near this transition region, there has not been a simple closed-form expression for V_T or E_T. In previous studies, V_T in β-Ga_2O_3 has been calculated

numerically,[24] but the dependence on the doping concentration, barrier height, and temperature is very complicated. Also, the non-monotonic temperature dependence of V_T is questionable. In this study, we first show from the numerical calculation that, unlike V_T, E_T is nearly *independent* of the doping concentration and the barrier height; furthermore, there exists a universal monotonic temperature dependence of E_T.

Experimentally, most of the previous analyses on the reverse leakage current in Ga_2O_3 SBDs use either the TE model[19,25] or the TFE model,[26,27] without considering their respective appropriate ranges. We have previous observed and verified near-ideal bulk reverse leakage current in Ga_2O_3 SBDs fabricated on bulk substrates.[20] However, due to the high doping concentration employed, the transition electric field could not be accessed in the study in Ref. 20. In this work, we fabricate SBDs on an n$^-$-Ga_2O_3 epitaxial layer, which allows us to access the surface electric field around E_T with the edge leakage current sufficiently suppressed with a field-plate structure.

For the calculation of the reverse leakage current, two effects on the shape of the Schottky barrier potential should be considered: image-force lowering (IFL) and doping effects, as illustrated schematically in Figs. 1(a) and 1(b), respectively. With both effects included, the potential energy distribution of the Schottky barrier under a surface electric field E is given by

$$\mathcal{E}_c(x) = e\phi_B - eEx - \frac{e^2}{16\pi\varepsilon_s x} + \frac{e^2(N_D - N_A)x^2}{2\varepsilon_s}, \quad (2)$$

where ϕ_B is the barrier height, $N_D - N_A$ is the net doping concentration, and $\varepsilon_s = 10\ \varepsilon_0$ is the dielectric constant of β-Ga_2O_3.[28] Here, the Fermi-level energy in metal ($\mathcal{E}_{Fm}$) is taken as the zero-energy level, as shown in Fig. 1(a). Due to the presence of IFL, the barrier is lowered

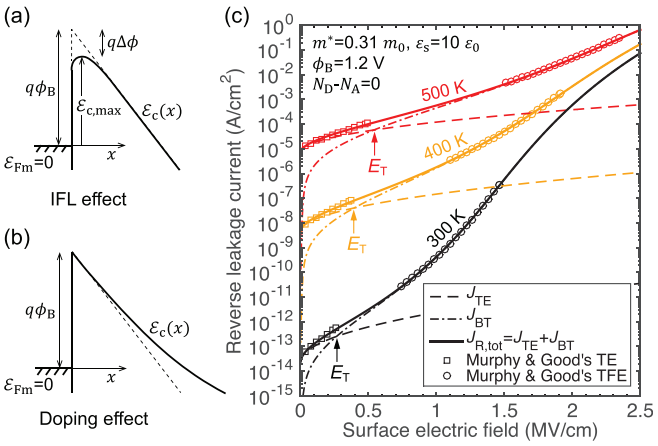

FIG. 1. Schematic illustrations of (a) the image-force lowering (IFL) effect (Reproduced with permission from Li *et al.*, Appl. Phys. Lett. **116**, 192101 (2020). Copyright 2020 AIP Publishing) and (b) the doping effect. (c) Calculated total reverse leakage current ($J_{R,tot}$) as a function of the surface electric field in Ga_2O_3 Schottky barrier diodes (SBDs) using our numerical model, showing excellent agreement with Murphy and Good's analytical models.[22] The transition electric field (E_T) is illustrated at the crossover point between the thermionic emission current (J_{TE}) and the barrier tunneling current (J_{BT}). It is worth noting that Murphy and Good's TE models actually include both the TE and BT currents despite what the name suggests, and thus, a match with $J_{R,tot}$ is observed, rather than with J_{TE}.

by $\Delta\phi = \sqrt{eE/(4\pi\varepsilon_s)}$, i.e., $\mathcal{E}_{c,max} = e(\phi_B - \Delta\phi)$. Assuming a transmission probability of unity for electrons with an energy $\mathcal{E}$ higher than $\mathcal{E}_{c,max}$, J_{TE} is given by the familiar expression,

$$J_{TE} = A^* T^2 \exp\left(-\frac{e\phi_B - e\Delta\phi}{k_B T}\right), \quad (3)$$

where $A^* = 4\pi m^* k_B^2 e/h^3$ is the Richardson constant.

On the other hand, including both IFL and doping effects in the calculation of the barrier tunneling current is analytically intractable, and thus, we developed a numerical approach, as presented in our previous work.[20] To obtain solely the barrier tunneling current, the upper limit of the integration in Ref. 20 should be changed to $\mathcal{E}_{c,max}$, i.e.,

$$J_{BT} = \frac{A^* T}{k_B}\int_{-\infty}^{\mathcal{E}_{c,max}} \mathcal{T}(\mathcal{E}) \cdot \ln\left[1 + \exp\left(-\frac{\mathcal{E} - \mathcal{E}_{Fm}}{k_B T}\right)\right] d\mathcal{E}, \quad (4)$$

where $\mathcal{T}(\mathcal{E})$ is the transmission probability, whose expression is given in Ref. 20. A single effective mass $m^* = 0.31\ m_0$ is adopted for both the Richardson constant and the tunneling effective mass in $\mathcal{T}(\mathcal{E})$ due to the single-valley and near-isotropic nature of the conduction band in β-Ga_2O_3.[29,30]

Figure 1 shows the calculated $J_{R,tot}$ using the numerical model and its constituent components (J_{TE}, J_{BT}). Here, we have temporality neglected the doping effect to compare with the analytical TE and TFE models derived by Murphy and Good,[22] which consider only the IFL. It can be seen that the calculated $J_{R,tot}$ from our numerical model agrees well with Murphy and Good's models within their respective applicable ranges, indicating that our numerical method is valid. It is worth noting that Murphy and Good's TE model actually includes both the TE and BT currents despite what the name suggests, and thus, it comes as no surprise that a match with $J_{R,tot}$ is observed, rather than with J_{TE}.

With the numerical model established, the transition electric field E_T can be calculated by equating J_{TE} with J_{BT}. Figure 2(a) shows the calculated E_T as a function N_D-N_A at different temperatures, at a barrier height of 1.2 eV. E_T is primarily a function of temperature and has a very weak dependence on N_D-N_A. It is nearly constant when N_D-$N_A < 10^{17}$ cm^{-3} and only increases slightly (<0.08 MV/cm) when N_D-N_A approaches 2×10^{18} cm^{-3}, indicating that the influence of the doping effect is near negligible. The surface electric field at zero bias (E_0) is also calculated by the familiar expression: $E_0 = \sqrt{2(N_D - N_A)(eV_{bi,0} - k_B T)/\varepsilon_s}$, where $V_{bi,0}$ is the built-in potential at zero bias. If E_0 is larger than E_T, $J_{R,tot}$ would be dominated by barrier tunneling, as in the case of the SBD we reported in Ref. 20. This illustrates the superiority of using the surface electric field instead of the reverse bias as the variable to characterize the transition region, as V_T would have a large dependence on N_D-N_A even with a constant E_T.

Knowing the weak dependence on the doping concentration, we calculate E_T as a function of temperature without considering the doping effect, as shown in Fig. 2(b). Here, we examine the influence of the barrier height ranging from 0.5–2.0 eV. Interestingly, there is a negligible dependence on the barrier height from 100 K to 800 K. This is because near the transition electric field, the majority of contribution to J_{BT} arises from the tunneling electrons with energy $\mathcal{E}$ close to $\mathcal{E}_{c,max}$, such that the natural log term in Eq. (4) can be simply replaced by $\exp\left(-\frac{\mathcal{E}-\mathcal{E}_{Fm}}{k_B T}\right)$, as long as the barrier height is not too small.

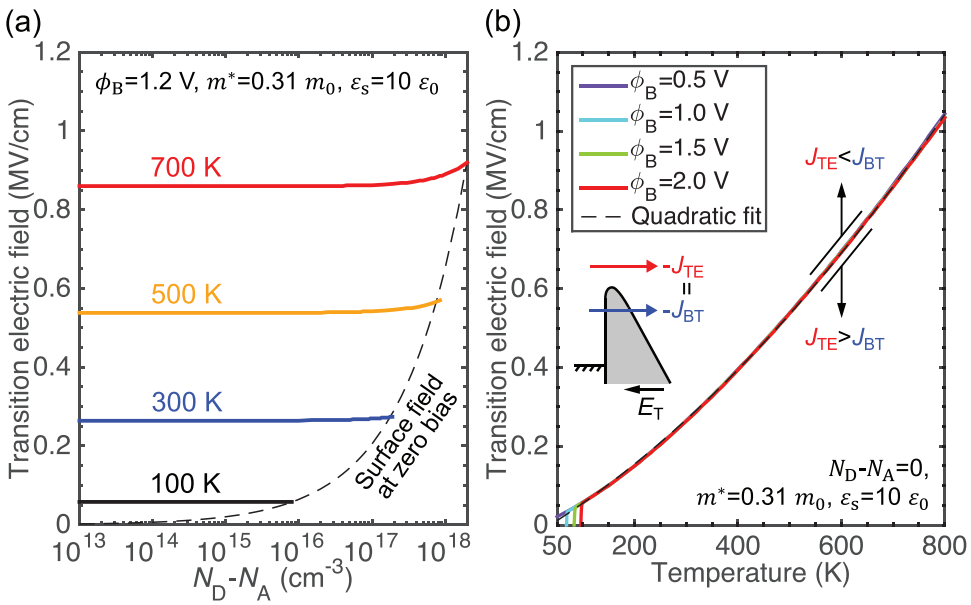

FIG. 2. Calculated transition electric field (E_T) in β-Ga_2O_3 SBDs as a function of (a) the net doping concentration (N_D-N_A) and (b) temperature.

Consequently, it can be shown that $J_{BT} \propto \exp(-e\phi_B/k_B T)$, and thus, the condition of $J_{BT} = J_{TE}$ does not depend on the barrier height. Below 100 K, however, there exists a sharp transition of E_T to zero at some "transition" temperature, depending on the barrier height. This comes from the fact that the contribution of tunneling electrons with energy $\mathcal{E}$ close to $\mathcal{E}_{Fm}$ can no longer be neglected, leading to more complicated dependence on the barrier height in J_{BT}. Because of the exponential decrease in J_{TE} at cryogenic temperatures, to match J_{BT} with J_{TE}, the required E_T is very low, <0.06 MV/cm. Also, with N_D-$N_A \geq 1 \times 10^{16}$ cm^{-3} in practice, the value of E_T around this transition region would already be lower than E_0, rendering it unobservable.

Due to the negligible dependence on the barrier height and very weak dependence on the doping concentration, we can describe E_T in β-Ga_2O_3 with a near-universal empirical temperature dependence as obtained from a quadratic fitting to the numerical calculation in Fig. 2(b),

$$E_T = 0.70 \cdot T^2 + 780 \cdot T - 3.0 \times 10^4 \text{ V/cm}, \quad (5)$$

where T is in units of K. Eq. (5) is valid within the temperature range of 100–800 K and a barrier-height range of 0.5–2.5 eV, with maximum errors of 0.01 MV/cm for N_D-$N_A \leq 1 \times 10^{17}$ cm^{-3} and 0.08 MV/cm for N_D-$N_A \leq 2 \times 10^{18}$ cm^{-3}.

To verify the existence of the transition region experimentally, we fabricated field-plated SBDs on a (001) Ga_2O_3 epitaxial wafer grown by halide vapor phase epitaxy (HVPE), as schematically shown in Fig. 3(a). The field plate length is designed to be 30 μm for the purpose of suppressing the electric field crowding at the anode edge. The cathode Ohmic contact is based on Ti/Au (50/100 nm), while the anode Schottky contact is based on Ni/Au (40/150 nm). The fabrication processes for the formation of cathode and anode contacts were the same as described in Ref. 31. After the anode formation, a 31 nm Al_2O_3 was deposited by atomic layer deposition (ALD) at 300 °C, acting as the dielectric for the field plate. Finally, a contact hole was etched, followed by the deposition of the field plate, which comprises a stack of Ni/Ti/Al/Pt (30/10/80/20 nm).

Temperature-dependent capacitance–voltage (C–V) measurements were performed on co-fabricated SBDs without the field plate. Figure 3(b) shows the extracted doping profile, which shows an average N_D-N_A value of $\sim 7 \times 10^{15}$ cm^{-3} in the Si-doped n$^-$ drift layer. The $1/C^2$-V plot is shown in the inset, from which the values of $V_{bi,0}$ are extracted to be 1.10 V at 25 °C and 0.92 V at 200 °C, corresponding to barrier heights of 1.27 eV and 1.21 eV, respectively (also see Figs. 4 and 7).

Figure 4(a) shows the measured temperature-dependent forward current–voltage (I–V) characteristics. Since the doping concentration is low, the depletion width at zero bias is ~ 0.4 μm. In this case, the TE model is inappropriate for the analysis of the forward I–V characteristics since the electron transport through the depletion region cannot be assumed ballistic, especially considering that the mobility of Ga_2O_3 is not very high.[3] Therefore, we analyze the data using the thermionic emission-diffusion (TED) model,[32,33] which considers the drift-

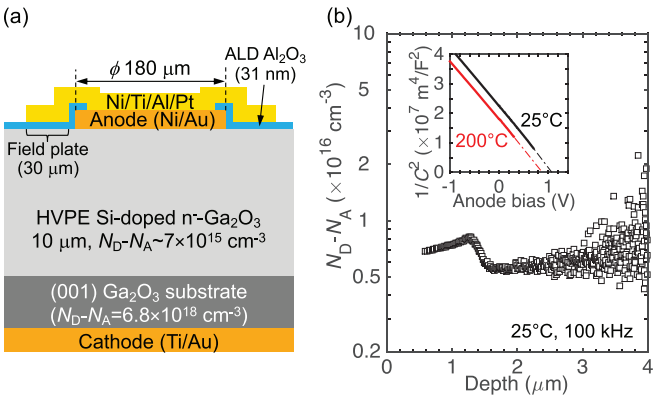

FIG. 3. (a) Schematic of the field-plated Ni-Ga_2O_3 SBDs fabricated on a HVPE Ga_2O_3 epitaxial wafer. (b) Extracted net doping concentration from C–V measurements on SBDs without the field plate. The inset shows the $1/C^2$–V plot that is used to extract the built-in potential at zero bias ($V_{bi,0}$).

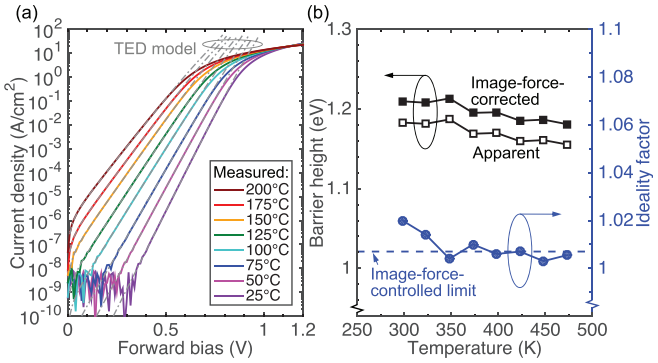

FIG. 4. (a) Temperature-dependent forward *I-V* characteristics of the Ga_2O_3 SBDs as well as the fitting using the thermionic emission-diffusion (TED) model. (b) Extracted barrier heights (apparent and image-force corrected values) as well as ideality factors as a function of temperature.

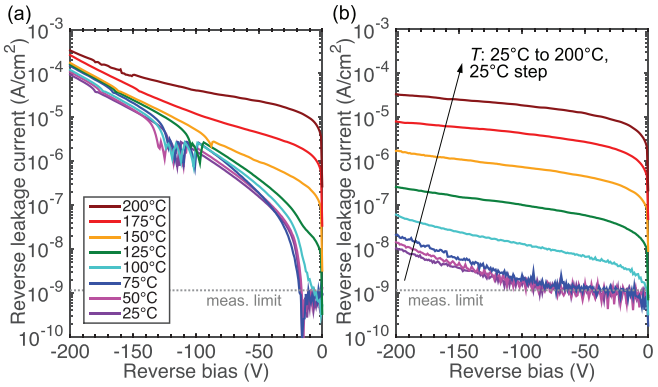

FIG. 5. Temperature-dependent reverse *I–V* characteristics on the Schottky barrier diodes (a) without the field plate, where the current below 100 °C is dominated by edge leakage arising from barrier tunneling beyond −20 V, and (b) with the field plate, where the contribution from edge tunneling is sufficiently suppressed above −200 V.

diffusion transport in the depletion region. In the calculations, the temperature-dependent drift mobility model in Ref. 3 is used with the Hall factor considered. The constant of proportionality is adjusted to match the Hall mobility of 145 $cm^2/V{\cdot}s$ measured at 25 °C on a similar wafer.[5]

The extracted barrier heights and ideality factors (n) from the TED model at each temperature are plotted in Fig. 4(b). The ideality factor is 1.02 at 25 °C and decreases to below 1.01 beyond 100 °C, indicating a very good Schottky contact quality. The image-force controlled ideality factor limit (n_{IF}) is calculated to be 1.007 using the standard method.[34] It can be seen that the extracted ideality factor approaches n_{IF} beyond 75 °C, further suggesting a near-ideal interface. Both the apparent barrier height and the barrier height after image-force (IF) correction (~0.026 eV)[34] were plotted. The IF-corrected barrier height is around 1.20 eV.

To verify the effect of the field plate in suppressing the edge leakage current, temperature-dependent reverse *I–V* measurements were performed on both non-field-plated and field-plated SBDs on the same wafer, as shown in Figs. 5(a) and 5(b), respectively. Without the field plate, the SBDs exhibit a large, near temperature-independent reverse leakage current below 100 °C. As have been pointed out in our previous report,[31] such a leakage behavior is characteristic of field-emission dominated edge leakage current due to electric-field crowding at the anode edge. On the other hand, the leakage current in SBDs with FP is much reduced, suggesting that the FP structure is effective in suppressing the edge electric-field crowding. Note that between −200 V and −100 V, there still exists a very low level of leakage current at 25–75 °C, which does not show a much temperature dependence, suggesting that there is still some edge leakage current not completely eliminated. However, considering the very low magnitude ($<10^{-8}$ A/cm^2) and the weak temperature dependence, it will not significantly "pollute" the uniform bulk leakage current from 100 °C to 200 °C, which we will model using our numerical models.

Figure 6 shows the temperature-dependent reverse leakage current as a function of the surface electric field, i.e., *J–E* characteristics. The reverse leakage characteristics from 100 °C to 200 °C can be well-fitted with the calculated *total* reverse leakage current ($J_{R,tot}$) using our numerical model [Eqs. (1)–(4)], *with the barrier height as the only fitting parameter at each temperature.* The individual components of $J_{R,tot}$, i.e., J_{TE} and J_{BT}, are also plotted in Fig. 6. While J_{TE} matches with the measured data at the lower end of E and J_{BT} at the higher end of E, neither J_{TE} nor J_{BT} alone can capture well the field dependence throughout the electric-field range (0.07–0.69 MV/cm). These results strongly suggest the presence of the transition regime, where both J_{TE} and J_{BT} are important.

The validity of the fitting depends critically on the fact that the measured bulk reverse leakage current is near ideal. A good check would be comparing the barrier height values extracted from the reverse leakage characteristics with those extracted from other methods. Figure 7 shows such comparisons. The barrier height values

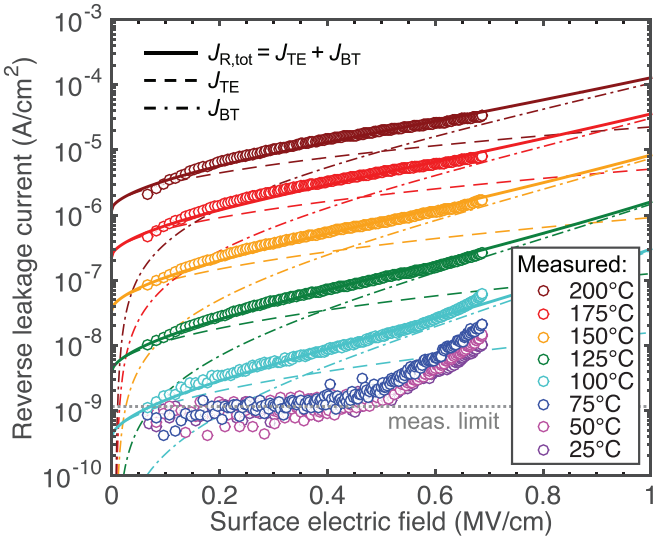

FIG. 6. Temperature-dependent reverse leakage current as a function of the surface electric field (*J–E* characteristics) in the field-plated Ga_2O_3 SBDs. The data are fitted with the calculated total reverse leakage current ($J_{R,tot}$) *with the barrier height as the only fitting parameter.* The constituent components, J_{TE} and J_{BT}, are also shown.

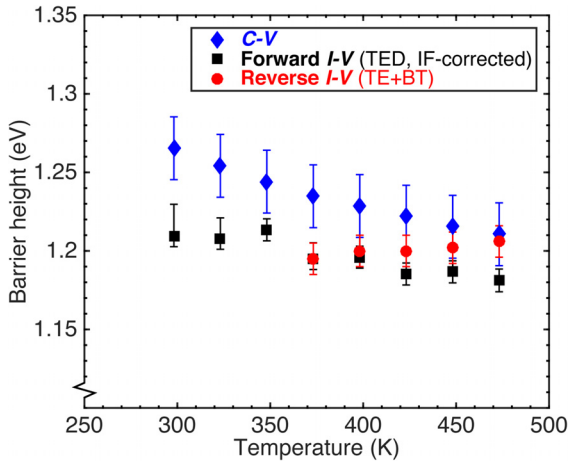

FIG. 7. Extracted barrier heights from *C–V* measurements, forward *I–V* measurements (using the TED model), and reverse *I–V* measurements (using our numerical leakage model considering both TE and BT).

extracted from forward *I–V*, reverse *I–V*, and *C–V* measurements exhibit good agreement. These provide further evidence that the measured reverse leakage current is near ideal, which, in turn, corroborates the identifications of the transition region from the data fitting in Fig. 6. The barrier heights extracted from *C–V* measurements are slightly larger than those from the *I–V* methods, especially at lower temperatures. This behavior is commonly observed (see, e.g., Ref. 19) and could be due to the presence of barrier height inhomogeneity[35] and/or uncertainty of the doping concentration close to the Schottky contact interface.

In conclusion, the transition electric field (E_T) separating the thermionic emission- and barrier tunneling-dominated reverse leakage regimes is calculated in β-Ga_2O_3 Schottky barrier diodes, by using a numerical reverse leakage model. E_T is shown to have a very weak dependence on the doping concentration and the barrier height. A near-universal empirical expression for E_T is obtained, which is valid for wide temperature, doping, and barrier-height ranges in β-Ga_2O_3 SBDs. Experimentally, we confirmed the presence of the transition region in field-plated Ga_2O_3 SBDs, which shows near-ideal bulk reverse leakage current well-matched with our numerical model. With the knowledge about the transition electric field, the long-standing confusion about whether the thermionic emission model or the tunneling model should be used is lifted: if the surface electric field is much lower than E_T, the thermionic emission model can be used; conversely, the barrier tunneling model should be employed. Near E_T, it is important to consider both models. These results and methodologies are highly valuable for the design of functional Schottky barriers in nearly all semiconductors that rely on the precise knowledge about the reverse leakage current.

This work was supported in part by ACCESS, an AFOSR Center of Excellence (No. FA9550-18-1-0529), and AFOSR (No. FA9550-20-1-0148) and was carried out at the Cornell Nanoscale Facility and CCMR Shared Facilities sponsored by the NSF NNCI program (No. ECCS-1542081), MRSEC program (No. DMR-1719875), and MRI No. DMR-1631282.

DATA AVAILABILITY

The data that support the findings of this study are available within this article.

REFERENCES

[1]M. Higashiwaki, K. Sasaki, A. Kuramata, T. Masui, and S. Yamakoshi, Appl. Phys. Lett. **100**, 013504 (2012).
[2]K. Ghosh and U. Singisetti, J. Appl. Phys. **124**, 085707 (2018).
[3]N. Ma, N. Tanen, A. Verma, Z. Guo, T. Luo, H. Xing, and D. Jena, Appl. Phys. Lett. **109**, 212101 (2016).
[4]A. Kuramata, K. Koshi, S. Watanabe, Y. Yamaoka, T. Masui, and S. Yamakoshi, Jpn. J. Appl. Phys., Part 1 **55**, 1202A2 (2016).
[5]K. Goto, K. Konishi, H. Murakami, Y. Kumagai, B. Monemar, M. Higashiwaki, A. Kuramata, and S. Yamakoshi, Thin Solid Films **666**, 182 (2018).
[6]M. Higashiwaki and G. H. Jessen, Appl. Phys. Lett. **112**, 060401 (2018).
[7]W. Li, Z. Hu, K. Nomoto, R. Jinno, Z. Zhang, T. Q. Tu, K. Sasaki, A. Kuramata, D. Jena, and H. G. Xing, in IEEE International Electron Devices Meeting (IEDM) (2018), p. 8.5.1.
[8]W. Li, K. Nomoto, Z. Hu, D. Jena, and H. G. Xing, IEEE Electron Device Lett. **41**, 107 (2020).
[9]J. Yang, F. Ren, M. Tadjer, S. J. Pearton, and A. Kuramata, ECS J. Solid State Sci. Technol. **7**, Q92 (2018).
[10]Z. Hu, K. Nomoto, W. Li, N. Tanen, K. Sasaki, A. Kuramata, T. Nakamura, D. Jena, and H. G. Xing, IEEE Electron Device Lett. **39**, 869 (2018).
[11]W. Li, K. Nomoto, Z. Hu, T. Nakamura, D. Jena, and H. G. Xing, in IEEE International Electron Devices Meeting (IEDM) (2019), p. 12.4.1.
[12]K. Tetzner, E. B. Treidel, O. Hilt, A. Popp, S. B. Anooz, G. Wagner, A. Thies, K. Ickert, H. Gargouri, and J. Würfl, IEEE Electron Device Lett. **40**, 1503 (2019).
[13]A. J. Green, K. D. Chabak, M. Baldini, N. Moser, R. Gilbert, R. C. Fitch, G. Wagner, G. Wagner, Z. Galazka, J. McCandless, A. Crespo, K. Leedy, and G. H. Jessen, IEEE Electron Device Lett. **38**, 790 (2017).
[14]Z. Xia, H. Xue, C. Joishi, J. Mcglone, N. K. Kalarickal, S. H. Sohel, M. Brenner, A. Arehart, S. Ringel, S. Lodha, W. Lu, and S. Rajan, IEEE Electron Device Lett. **40**, 1052 (2019).
[15]Q. He, W. Mu, B. Fu, Z. Jia, S. Long, Z. Yu, Z. Yao, W. Wang, H. Dong, Y. Qin, G. Jian, Y. Zhang, H. Xue, H. Lv, Q. Liu, M. Tang, X. Tao, and M. Liu, IEEE Electron Device Lett. **39**, 556 (2018).
[16]A. Takatsuka, K. Sasaki, D. Wakimoto, Q. T. Thieu, Y. Koishikawa, J. Arima, J. Hirabayashi, D. Inokuchi, Y. Fukumitsu, A. Kuramata, and S. Yamakoshi, in 76th Device Research Conference (DRC), pp. 1–2.
[17]T. Oishi, K. Urata, M. Hashikawa, K. Ajiro, and T. Oshima, IEEE Electron Device Lett. **40**, 1393 (2019).
[18]T. Oshima, T. Okuno, N. Arai, N. Suzuki, S. Ohira, and S. Fujita, Appl. Phys. Express **1**, 011202 (2008).
[19]C. Hou, R. M. Gazoni, R. J. Reeves, and M. W. Allen, IEEE Electron Device Lett. **40**, 1587 (2019).
[20]W. Li, D. Saraswat, Y. Long, K. Nomoto, D. Jena, and H. G. Xing, Appl. Phys. Lett. **116**, 192101 (2020).
[21]D. Saraswat, W. Li, K. Nomoto, D. Jena, and H. G. Xing, in Device Research Conference (DRC), pp. 1–2.
[22]E. L. Murphy and R. H. Good, Jr., Phys. Rev. **102**, 1464 (1956).
[23]F. A. Padovani and R. Stratton, Solid State Electron. **9**, 695 (1966).
[24]A. Latreche, Semicond. Phys. Quantum Electron. Optoelectron. **22**, 397 (2019).
[25]K. Konishi, K. Goto, H. Murakami, Y. Kumagai, A. Kuramata, S. Yamakoshi, and M. Higashiwaki, Appl. Phys. Lett. **110**, 103506 (2017).
[26]M. Higashiwaki, K. Konishi, K. Sasaki, K. Goto, K. Nomura, Q. T. Thieu, R. Togashi, H. Murakami, Y. Kumagai, B. Monemar, A. Koukitu, A. Kuramata, and S. Yamakoshi, Appl. Phys. Lett. **108**, 133503 (2016).
[27]B. Wang, M. Xiao, X. Yan, H. Y. Wong, J. Ma, K. Sasaki, H. Wang, and Y. Zhang, Appl. Phys. Lett. **115**, 263503 (2019).
[28]B. Hoeneisen, C. A. Mead, and M.-A. Nicolet, Solid State Electron. **14**, 1057 (1971).
[29]H. Peelaers and C. G. Van de Walle, Phys. Status Solidi B **252**, 828 (2015).
[30]Y. Zhang, A. Neal, Z. Xia, C. Joishi, J. M. Johnson, Y. Zheng, S. Bajaj, M. Brenner, D. Dorsey, K. Chabak, G. Jessen, J. Hwang, S. Mou, J. P. Heremans, and S. Rajan, Appl. Phys. Lett. **112**, 173502 (2018).

[31]W. Li, K. Nomoto, Z. Hu, D. Jena, and H. G. Xing, in Device Research Conference (DRC), pp. 159–160.
[32]S. M. Sze and K. K. Ng, *Physics of Semiconductor Devices*, 3rd ed. (Wiley, New York, 2007), pp. 159–162.
[33]T. Maeda, M. Okada, M. Ueno, Y. Yamamoto, T. Kimoto, M. Horita, and J. Suda, Appl. Phys. Express **10**, 051002 (2017).
[34]W. Mönch, J. Vac. Sci. Technol., B **17**, 1867 (1999).
[35]J. H. Werner and H. H. Güttler, J. Appl. Phys. **69**, 1522 (1991).